Mechanical properties of defective single wall carbon nanotubes

Yaroslav V. Shtogun[a] and Lilia M. Woods
Department of Physics, University of South Florida, Tampa, Florida 33620, USA

(Received 31 December 2008; accepted 4 April 2009; published online 26 March 2010)

First principle density functional theory calculations for radially deformed and defective single wall (8,0) carbon nanotube are reported. Structural changes in terms of radial cross-sectional geometry and bond length changes are studied for different values of the applied strain for all types of investigated deformations and defects. Various characteristic deformation and defect energies are shown as a function of the applied deformation. The nonlinear elastic properties of the radially deformed and defective (8,0) nanotube are also investigated in terms of the strain energy and applied force. © *2010 American Institute of Physics*. [doi:10.1063/1.3340519]

I. INTRODUCTION

Carbon nanotubes (CNTs) are quasi-one-dimensional (1D) infinite graphene sheets rolled up into cylinders.[1] They have drawn a great deal of interest because of their unique properties and potential applications. Nowadays, many studies are devoted to outstanding mechanical properties of CNTs, such as their high elastic modulus, strength, flexibility, and low mass density. CNTs also show reversible deformation in a wide range of elastic bending, buckling, and torsion, which makes them a key element for polymer composites and nanodevices.[2–6] The quasi-1D tubular structure makes them practically incompressible in the axial direction, while the radial direction is much more flexible. It has been shown that radial deformation takes place in bundles of CNTs due to van der Waals interaction,[7,8] or under applied hydrostatic pressure[9,10] or after squeezing the nanotube by an atom force microscopy (AFM) tip.[11,12] The radial deformation of single wall CNTs changes not only their mechanical but also their electronic properties. It has been reported in previous studies, that CNTs can experience metal-semiconductor transitions and reduction in their conductance upon radial deformation.[13–16]

The CNT mechanical and electronic structure properties can also be modified by the presence of various defects, which can appear during the CNT growth, purification, or device production processes. For example, Stone–Wales (SW) defects reduce the CNT quantum conductance and increase their reactivity upon adsorption of different molecules and atoms.[17,18] Impurities, such as boron or nitrogen atoms, create donor or acceptor levels in the band structure, break the mirror symmetry, shift the Fermi level, and improve reactivity to other compounds.[17,19–21] Furthermore, vacancies can cause significant changes in electronic, mechanical, and magnetic properties of CNT as well.[22–26] In many instances, however, CNT are subject to radial deformations and defects at the same time. Since all synthesized nanotubes have some degree of defects, radially squeezing them may lead to different changes in the electronic and mechanical structure. Moreover, intentionally creating defects on already deformed CNT has been used as an additional way to control their properties.[27,28]

Being the strongest and stiffest among man made materials, CNTs are expected to have a key role when strong nanostructured materials are required. Therefore, better understanding and characterization of their mechanical properties are needed. The elastic moduli of CNTs were measured in several experiments using different methods, such as transmission electron microscopy or AFM.[29–31] The reported values for the Young's modulus vary greatly in the range $0.1 \div 2.0$ TPa. These values can be affected by changes in the environmental temperature, applied load, or measurement technique. Calculations based on first principle methods have also been carried out to determine their mechanical characteristics such as the elastic constants, Poisson's ratio and Young's modulus.[24,25,32–39] Although *ab initio* calculations are quite reliable, they can be very intensive since they require large amounts of computer resources. At the same time, continuum mechanics is relatively easy to apply, it does not require supercomputers, and it has shown reasonable success in describing CNT mechanical properties.

This work investigates the structural and mechanical properties of the radially deformed and defective semiconducting (8,0) CNT under large radial deformation. We consider two types of radial deformations by applying different loads, one – narrower than the tube's cross-section and the other – wider than the tube's cross-section. The first type corresponds to deformations with a narrow tip or between two narrow hard surfaces, while the second one corresponds to deformations with a wider tip or between two infinite hard surfaces. Also, three isolated defects are studied – a SW defect, a nitrogen (N) impurity, and a monovacancy (MV) located at the highest nanotube curvature.

We perform first principle total energy calculations and analyze the nanotube structural changes in terms of the type and degree of radial deformation and type of the present defect. The energy needed to deform the nanotube as well as the energies needed to form each defect are examined as a function of radial deformation. We also discuss the relationship between the deformation energy and applied strain in order to connect the *ab initio* results with an appropriate

[a]Electronic mail: yshtogun@cas.usf.edu.

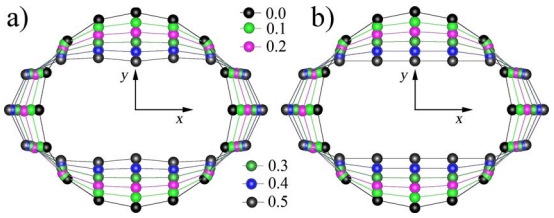

FIG. 1. (Color online) The cross-sectional transformation of (8,0) CNT from circular through elliptical to (a) peanut structure and (b) flat structure at different degree of radial deformation.

continuum mechanics description. The nonlinear response of the nanotube is analyzed in term of applied strain, strain energies, and applied force.

The paper is organized as follows. The computational method and model for radial deformation of defective CNTs are described in Sec. II. The geometry changes, characteristic energies, and mechanical properties with appropriate discussions are presented in Sec. III. The conclusions are given in Sec. IV.

II. COMPUTATIONAL METHOD AND MODEL

The presented calculations for the various structural and energy dependences are performed based on self-consistent density functional theory (DFT) within the local density approximation for the exchange-correlation functional implemented in the VASP package.[40] This code uses a plane-wave basis set and a periodic supercell method. The core electrons are treated either by utilizing ultrasoft Vanderbilt pseudopotentials or by the projector-augmented wave method.[41] In our calculations we use ultrasoft pseudopotentials method. The $(1\times1\times7)$ Monkhorst–Pack k-grid is utilized for Brillouin zone integration with an energy cut-off of 420 eV for all systems. Also, the relaxation criteria for all systems are 10^{-5} eV for the total energy and 0.005 eV/Å for the total force. The constructed supercell for the zigzag (8,0) nanotube consists of four unit cells along the z-axis of the nanotube and it has dimensions $(22.12\times22.12\times17.03)$ Å^3 after relaxation. This supercell size is large enough and it avoids interactions between neighboring nanotubes and also simulates isolated defects in the nanotube network. For the (8,0) nanotube with a N impurity and MV spin polarization effects are included due to the unpaired electron or uncoordinated carbon atom in each defective structure, respectively. Our calculations correspond to first applying radial deformation to the CNT and then creating a defect at the highest curvature of the nanotube.

A. Radial deformation

The radial deformation in our study is created by applying stress σ_{yy} along the y-axis on the surface of the nanotube – Fig. 1. Consequently, the diameter is squeezed in the y-direction and elongated in the x-direction. Two types of radial deformation are simulated – one between two narrow hard walls (wall size $\sim$1.5 Å), and one between two infinitely wide hard walls. To characterize the radial squeezing, we use the applied strains along the x-axis and y-axis

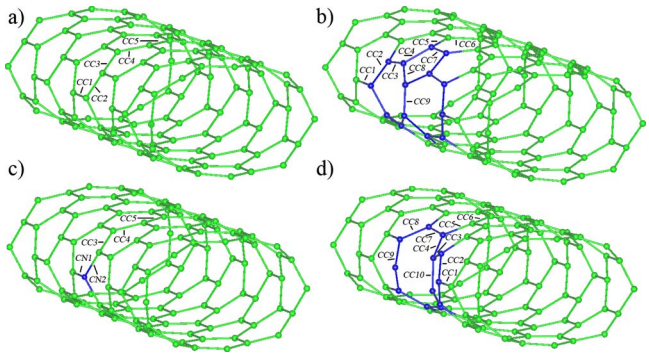

FIG. 2. (Color online) The relaxed structure of (8,0) CNT at $\epsilon_{yy}=0.25$ with (a) no defect; (b) SW defect; (c) N impurity; (d) MV. The bonds on the highest curvature region are denoted.

$$\epsilon_{xx}=\frac{D_0-a}{D_0}, \tag{1}$$

$$\epsilon_{yy}=\frac{D_0-b}{D_0}, \tag{2}$$

where D_0 is the diameter of the undeformed nanotube, a is major axis connecting the highest curvature regions (along y), and b is the minor axis connecting the lowest curvature regions (along x). In the case of the narrower deformation, the y-coordinates of the top and bottom rows at the lowest curvature are fixed, and all other coordinates are let free. In the case of the wider deformation, the y-coordinates of the atoms from the top and bottom flat regions are kept fixed. Here, we study the radial deformation in $0\leq\epsilon_{yy}\leq0.5$ range for both types of deformation.

In Fig. 1 we show the results for the relaxed structure of the deformed (8,0) CNT. One sees that for small deformation $\epsilon_{yy}<0.35$, both types of deformations show little difference and the nanotube cross-section is elliptical-like. For $\epsilon_{yy}>0.35$, however, the narrower squeezing results in a peanut-like structure, while the wider squeezing results in a flat-like structure. The peanut one is indented on the top and bottom of the y-axis, while the flat one has two flat parts along the x-axis. Allowing all coordinates to relax restores the original circular cross-section of (8,0) CNT, indicating that these types of deformations are elastic.

B. Defects on the deformed (8,0) CNT

After the (8,0) CNT is deformed and relaxed, a single defect is created at one of the highest curvature regions as shown in Fig. 2. The structures are relaxed again by keeping the appropriate constraints for the radial deformation, as described earlier. We consider a SW defect created by rotating one C–C bond (Fig. 2(b)), a N impurity by substituting one C atom (Fig. 2(c)), and a MV by removing one C atom (Fig. 2(d)) from the nanotube network. The vacancy creation in the CNT structure leads to the formation of several metastable MV configurations.[42] The most stable MV for the zigzag (8,0) CNT is shown in Fig. 2(d), where the created nonagon and pentagon of MV are along the nanotube axis. For a defective nanotube the applied strains ϵ_{xx} and ϵ_{yy} are also calculated using Eqs. (1) and (2). However, a of the

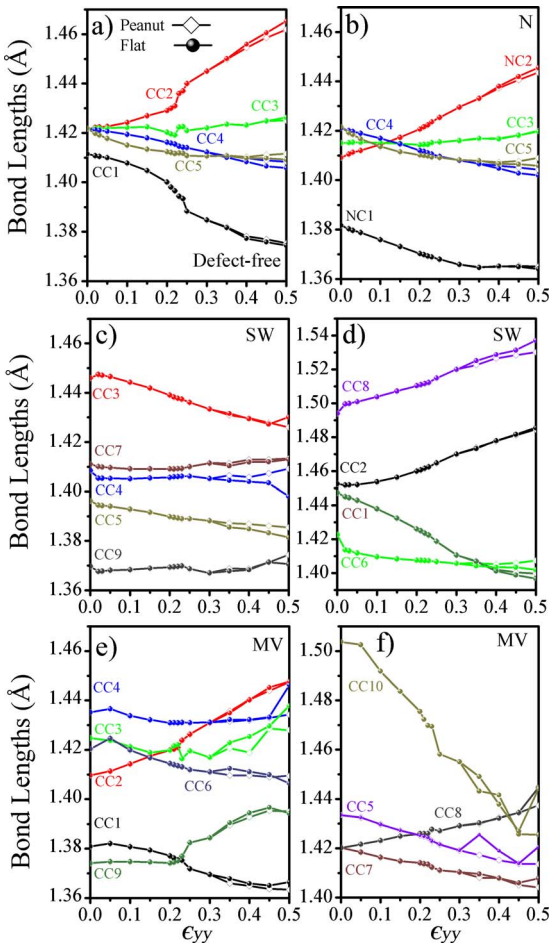

FIG. 3. (Color online) Bond lengths as a function of deformation for (a) a defect-free (8,0) CNT; (b) (8,0) CNT with a N impurity; (c) and (d) (8,0) CNT with a SW; (e) and (f) (8,0) CNT with a MV defect.

deformed-defective nanotubes is measured along x-axis as the distance from the defect to the opposite side of the nanotube for ϵ_{xx}. For example, the measured distance for the (8,0) CNT with the SW defect is between $CC9$ bond and the opposite site of the tube; the measured distance for the (8,0) CNT with N is between the N atom and the opposite nanotube site, and the measured distance for the (8,0) CNT with MV is between $CC10$ and the opposite site (Fig. 2). Releasing all coordinates restores the circular form of the nanotube with the defect on its surface, thus the tube is elastic regardless of the defects present.

III. RESULTS AND DISCUSSION

A. Structural changes in the deformed and defective CNT structure

We first present results for the structural changes in the deformed and defective tubes. Figure 2 shows the relaxed structure for the radial deformation $\epsilon_{yy}=0.25$ for all studied defects. Also, Fig. 3 shows the evolution of several C–C bonds for the defect free CNT as well as the C–C bonds involved in the defects (denoted on Fig. 2) as a function of applied strain. Figure 3(a) indicates that the $CC1$ and $CC2$ located at the highest curvature region experience the most significant changes as the CNT is squeezed. The $CC1$ bond decreases by 0.04 Å, while the $CC2$ bond increases by 0.05 Å for $\epsilon_{yy}=0.0\div0.5$. The presence of the N atom does not disturb significantly the CNT structure and similar behavior is found for the CNT with N impurity (Fig. 3(b)). However, due to the larger size of the N atom, the studied bond lengths are smaller as compared to the defect-free CNT.

The bond length changes involving the SW defect are shown on Figs. 3(c) and 3(d). Again, the $CC1$, $CC2$, and $CC8$ bonds situated at the highest curvature are the ones that show most significant changes as a function of ϵ_{yy}. The C–C bonds for the CNT with a MV show most dramatic changes (Figs. 3(e) and 3(f)). In particular, the $CC10$ decreases by 0.08 Å, while the $CC9$ increases by 0.03 Å, and $CC2$ increases by 0.04 Å for $\epsilon_{yy}=0.0\div0.5$. One also notices that several of the bonds show discontinuous functional dependence as a function of ϵ_{yy}, while for the N and SW defects all bonds are rather smooth.

Figures 2 and 3 indicate that there is practically no difference in the deformed CNT structure for both types of deformation until $\epsilon_{yy}=0.35$. After that, small changes are found for all cases, except for the CNT with MV, for which there are larger deviations for several of the C–C distances.

B. Energetics of the deformed and defective CNT

We further calculate the different deformation and defect formation energies. The energy needed to deform a defect-free CNT E^f_η and the energies needed to create the different defects $E^f_{\eta/\mathrm{Defect}}$ are calculated as follows:

$$E^f_\eta = E_\eta - E, \tag{3}$$

$$E^f_{\eta/\mathrm{SW}} = E_{\eta/\mathrm{SW}} - E_\eta, \tag{4}$$

$$E^f_{\eta/\mathrm{N}} = E_{\eta/\mathrm{N}} - E_\eta - \mu_\mathrm{N} + \mu_\mathrm{C}, \tag{5}$$

$$E^f_{\eta/\mathrm{MV}} = E_{\eta/\mathrm{MV}} - E_\eta + \mu, \tag{6}$$

where E_η – the total energy for the deformed CNT, E – the total energy for the undeformed perfect CNT, $E_{\eta/\mathrm{SW,N,MV}}$ – the total energies for the deformed CNT with the appropriate defect, $\mu_{\mathrm{N,C}}$ – the chemical potentials for a free nitrogen and carbon atoms, respectively, and μ – the chemical potential of a carbon atom in the nanotube as an energy per C atom.

In Fig. 4, we show how E^f_η and $E_{\eta/\mathrm{SW,N,MV}}$ evolve as a function of the applied strain ϵ_{yy}. The deformation energy for the defect-free CNT increases nonlinearly as the strain is increased. This increase is larger for the flat CNT as compared to the peanut one ($\epsilon_{yy}>0.35$).

It appears that it costs more energy to create a MV on the (8,0) CNT ($E^f_{\eta/\mathrm{MV}}=5.43$ eV) as compared to creating a N impurity ($E^f_{\eta/\mathrm{N}}=3.26$ eV) or a SW defect ($E^f_{\eta/\mathrm{SW}}=3.02$ eV) at $\epsilon_{yy}=0.0$. This follows from the fact, that the MV introduces much bigger disturbance in the CNT and it requires breaking three carbon bonds to form one MV defect. For all studied cases, the defect-formation energy decreases nonlinearly as a function of ϵ_{yy}, indicating that it is easier to form the defect on already deformed nanotube. This decrease is the largest for the MV – 1.43 eV. Substituting a N atom in the (8,0) CNT does not change $E^f_{\eta/\mathrm{N}}$ for $\epsilon_{yy}>0.25$ and the

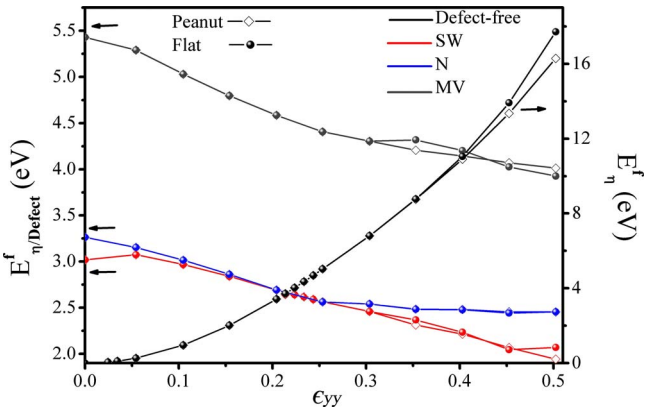

FIG. 4. (Color online) Deformation and defect formation energies as a function of applied strain ϵ_{yy} for peanut and flat (8,0) CNT structures.

changes in $E^f_{\eta/N}$ is ~0.81 eV. Apparently, rotating a C–C bond on highly deformed CNTs is the easiest process since $E^f_{\eta/SW} \approx 0.2$ eV is the smallest at $\epsilon_{yy}=0.5$, while the changes in $E^f_{\eta/SW}$ is ~1.00 eV. There is also little difference in energy for flat and peanut tube, except some small deviations for the SW and MV defects for $\epsilon_{yy} > 0.35$.

C. Elastic properties of the (8,0) CNT

Here we discuss the elastic properties of the deformed (8,0) CNT. The generalized Hook's law for nonlinear elasticity gives the relation between the applied stress σ_{ij} and the strain ϵ_{ij} in the system as follows:

$$\sigma_{ij} = C_{ijkl}\epsilon_{ij} + C_{ijklmn}\epsilon_{ij}\epsilon_{mn}, \tag{7}$$

where C_{ijkl} and C_{ijklmn} are the second and third order elastic constants, σ_{ij} is the stress tensor, and ϵ_{ij} is the strain tensor. There is no applied stress along the x-direction, therefore, for the CNT one obtains:

$$\sigma_{xx} = C_{11}\epsilon_{xx} + C_{12}\epsilon_{yy} + C_{111}\epsilon_{xx}^2 + 2C_{112}\epsilon_{xx}\epsilon_{yy} + C_{122}\epsilon_{yy}^2 = 0, \tag{8}$$

where we have used the contracted Voight notation for the indexes in C_{iikl} and C_{iikkmm} as $C_{\alpha\beta}$ and $C_{\alpha\beta\gamma}$, respectively.[43] The solution of the quadratic Eq. (8) gives $\epsilon_{xx}=f(\epsilon_{yy})$. Taking Taylor expansion with respect to the parameter $\epsilon_{yy} < 1.0$, we find the approximate expression

$$-\epsilon_{xx} = \nu\epsilon_{yy} + \xi\epsilon_{yy}^2, \tag{9}$$

where

$$\nu = \frac{C_{12}}{C_{11}}, \tag{10}$$

is the Poisson's ratio and

$$\xi = \frac{C_{11}^2(C_{112}^2 - C_{111}C_{122}) - (C_{11}C_{112} - C_{12}C_{111})^2}{C_{11}^3 C_{111}}, \tag{11}$$

is the nonlinear contribution. The calculated results for ϵ_{xx} versus ϵ_{yy} are given in Figs. 5(a) and 5(b). Performing polynomial regression analysis, we can estimate the values of the constants ν and ξ (given in Table I). Figures 5(a) and 5(b) show that there is very good agreement between the *ab initio* results and the regression analysis curves for the (8,0) CNT with or without defects.

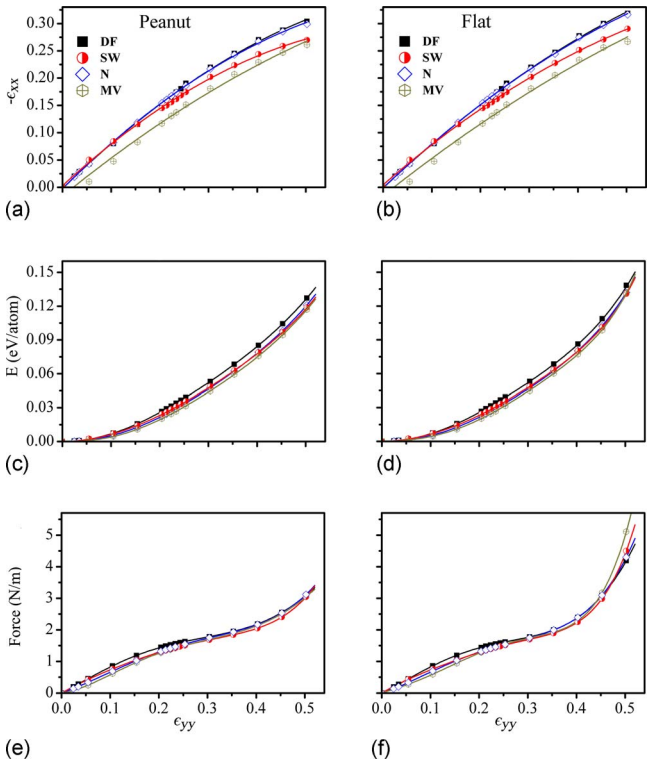

FIG. 5. (Color online) (a) and (b) Nonlinear response of strain ϵ_{xx}, (c) and (d) strain energy changes per atom, (e) and (f) applied forces on the CNT surface for peanut and flat deformations in defect-free and defective (8,0) CNT, respectively, as a function of the applied strain ϵ_{yy}. The dots are DFT calculated data and the lines show the regression fitting analysis.

One finds that the Poisson ratio and the absolute value of the nonlinear term are always larger for the peanut CNT as compared to the flat one for all cases. Also ν for the defect-free CNT is the largest, while ν for the CNT with a MV is the smallest. The same is true for $|\xi|$, except for SW and N, where $|\xi|$ have similar values as the defect-free nanotube.

The energy change per atom as a function of applied strain can also be obtained using classical theory of elasticity. Using the generalized Hooke's law, the energy change per atom $\Delta E=[E(\epsilon_{xx},\epsilon_{yy})-E(0,0)]/N$, with N being the number of atom in the supercell, is[44]

$$\Delta E = \frac{1}{2}\sum_{ijkl} C_{ijkl}\epsilon_{ij}\epsilon_{kl} + \frac{1}{6}\sum_{ijklmn} C_{ijklmn}\epsilon_{ij}\epsilon_{kl}\epsilon_{mn} + \ldots. \tag{12}$$

For the radial deformation of CNTs there are only two components of ϵ_{ij} such as ϵ_{xx} and ϵ_{yy}. Thus, substituting Eq. (9) into Eq. (12) one obtains ΔE as a function of ϵ_{yy}

$$\Delta E \cong A_2\epsilon_{yy}^2 + A_3\epsilon_{yy}^3 + A_4\epsilon_{yy}^4 + A_5\epsilon_{yy}^5 + A_6\epsilon_{yy}^6 + O(\epsilon_{yy}^7), \tag{13}$$

where the A_n for $n=2\div6$ contain combinations of the second-order and third-order elastic constants. In Figs. 5(c) and 5(d) we show the calculated results for ΔE as well as the polynomial regression analysis using Eq. (13). The agreement is very good. The fitting constants A_n are calculated and

TABLE I. The regression analysis data for the fitting parameters: ν, ξ, and ΔE.

	Defect-free		SW		N		MV	
	Peanut	Flat	Peanut	Flat	Peanut	Flat	Peanut	Flat
ν	0.875	0.842	0.82	0.775	0.884	0.845	0.727	0.709
ξ	−0.512	−0.393	−0.564	−0.41	−0.552	−0.417	−0.323	−0.257
$A_2(J/m^2)$	3.916	3.684	4.362	4.758	2.623	2.440	0.921	2.312
$A_3(J/m^2)$	5.697	8.686	−6.466	−12.761	8.003	10.224	22.167	1.000
$A_4(J/m^2)$	−40.577	−52.924	19.307	55.833	−29.829	−38.046	−81.179	34.142
$A_5(J/m^2)$	67.307	82.795	−49.666	−141.685	30.433	36.600	116.754	−150.261
$A_6(J/m^2)$	−31.305	−28.938	49.953	136.433	−0.738	9.077	−55.571	169.641

listed in Table I. ΔE displays similar values and similar behavior for the deformed (8,0) CNT with or without defects.

The force per unit circumference applied to the radial direction along y-axis is the first derivative of the ΔE

$$F = \frac{\partial \Delta E}{\partial \epsilon_{yy}} = 2A_2\epsilon_{yy} + 3A_3\epsilon_{yy}^2 + 4A_4\epsilon_{yy}^3 + 5A_5\epsilon_{yy}^4 + 6A_6\epsilon_{yy}^5. \tag{14}$$

The dependence of F as a function of the ϵ_{yy} strain is shown in Figs. 5(e) and 5(f). There is very little difference between the force to deform a defect-free or a defective nanotube. The variation in F is very close to linear for $\epsilon_{yy} < 0.20$. In the $0.2 < \epsilon_{yy} < 0.3$ for the peanut as well as for the flat CNT regions, the curve changes its slope becoming more flat. This is an indication of the onset of the nonlinear contribution to F. After that the force functionality changes its slope again showing a steep increase as ϵ_{yy} becomes larger. This behavior is much more pronounced for the flat (8,0) CNT. Thus larger force is needed to deform the CNT into a flat shape as compared to the force needed to deform the nanotube into a peanut one.

IV. CONCLUSIONS

In conclusion, we have reported first-principal calculations based on DFT to study properties of a radially deformed and defective (8,0) CNT related to its structure, energetics, and elasticity. We find that the C–C bonds located on the highest curvature of the CNT as well as the ones comprising the SW, N, or MV defects are the ones that exhibit the most significant changes as a function of radial strain. The energy to deform the nanotube is very similar in values for both deformations at smaller strain and it is higher for the flat deformation than the peanut one for larger stain. We find that the defect formation energy decreases as the deformation increases for all defects, however, $E^f_{\eta/\mathrm{MV}}$ is significantly larger than $E^f_{\eta/\mathrm{N}}$ and $E^f_{\eta/\mathrm{SW}}$. Finally, the nonlinear elastic properties of the (8,0) nanotube are also studied using the Hooke's law continuous model. We were able to obtain very good agreement between the *ab initio* calculated results and polynomial regression analysis fitting by taking a quadratic nonlinear term in the ϵ_{xx} versus ϵ_{yy} relationship. The elastic energy per atom and the force necessary to deform the tube show large nonlinear contributions at $\epsilon_{yy} > 0.2$ for all cases. The presences of defects in the nanotube structure decrease the Poisson's ratio and nonlinear coefficient as compared to the defect-free nanotube.

ACKNOWLEDGMENTS

We would like to acknowledge the use of the services and support provided by the Research Computing Core at the University of South Florida, the TeraGrid Advanced Support Program at the University of Illinois, and the High Performance Computing facilities of DoD.

[1] R. Saito, G. Dresselhaus, and M. S. Dresselhaus, *Physical Properties of Carbon Nanotubes* (Imperial College, London, 1998).
[2] M. R. Falvo, G. J. Clary, R. M. Taylor, V. Chi, F. P. Brooks, S. Washburn, and R. Superfine, Nature (London) **389**, 582 (1997).
[3] M. Griebel and J. Hamaekers, Comput. Methods Appl. Mech. Eng. **193**, 1773 (2004).
[4] P. M. Ajayan, L. S. Schadler, S. C. Giannaris, and A. Rubio, Adv. Mater. **12**, 750 (2000).
[5] A. R. Hall, M. R. Falvo, R. Superfine, and S. Washburn, Nat. Nanotechnol. **2**, 413 (2007).
[6] T. Cohen-Karni, L. Segev, O. Srur-Lavi, S. R. Cohen, and E. Joselevich, Nat. Nanotechnol. **1**, 36 (2006).
[7] R. S. Ruoff, J. Tersoff, D. C. Lorents, S. Subramoney, and B. Chan, Nature (London) **364**, 514 (1993).
[8] T. Hertel, R. E. Walkup, and P. Avouris, Phys. Rev. B **58**, 13870 (1998).
[9] J. Tang, L.-C. Qin, T. Sasaki, M. Yudasaka, A. Matsushita, and S. Iijima, Phys. Rev. Lett. **85**, 1887 (2000).
[10] S. A. Chesnokov, V. A. Nalimova, A. G. Rinzler, R. E. Smalley, and J. E. Fischer, Phys. Rev. Lett. **82**, 343 (1999).
[11] I. Palaci, S. Fedrigo, H. Brune, C. Klinke, M. Chen, and E. Riedo, Phys. Rev. Lett. **94**, 175502 (2005).
[12] M. Minary-Jolandan and M.-F. Yu, Appl. Phy. **103**, 073516 (2008).
[13] A. P. M. Barboza, A. P. Gomes, B. S. Archanjo, P. T. Araujo, A. Jorio, A. S. Ferlauto, M. S. C. Mazzoni, H. Chacham, and B. R. A. Neves, Phys. Rev. Lett. **100**, 256804 (2008).
[14] B. Shan, G. W. Lakatos, S. Peng, and K. Cho, Appl. Phys. Lett. **87**, 173109 (2005).
[15] E. D. Minot, Y. Yaish, V. Sazonova, J.-Y. Park, M. Brink, and P. L. McEuen, Phys. Rev. Lett. **90**, 156401 (2003).
[16] V. H. Crespi, M. L. Cohen, and A. Rubio, Phys. Rev. Lett. **79**, 2093 (1997).
[17] H. J. Choi, J. Ihm, S. G. Louie, and M. I. Chohen, Phys. Rev. Lett. **84**, 2917 (2000).
[18] C. Wang, G. Zhou, K. Liu, J. Wu, Y. Qiu, B.-L. Gu, and W. Duan, J. Phys. Chem. B **110**, 10266 (2006).
[19] T. Koretsune and S. Saito, Phys. Rev. B **77**, 165417 (2008).
[20] S. H. Lim, R. Li, W. Ji, and J. Lin, Phys. Rev. B **76**, 195406 (2007).
[21] A. H. Nevidomskyy, G. Csanyi, and M. C. Payne, Phys. Rev. Lett. **91**, 105502 (2003).
[22] A. J. Lu and B. C. Pan, Phys. Rev. Lett. **92**, 105504 (2004).
[23] G. Kim, B. M. Jeong, and J. Ihm, Appl. Phys. Lett. **88**, 193107 (2006).
[24] Y. Shi-Jun, K. Yong, and L. Fa-Shen, Chin. Phys. Lett. **24**, 2036 (2007).
[25] M. Sammalkorpi, A. Krasheninnikov, A. Kuronen, K. Nordlund, and K. Kaski Phys. Rev. B **70**, 245416 (2004).
[26] W. Orellana and P. Fuentealbe, Surf. Sci. **600**, 4305 (2006).

[27]S. B. Fangan, L. B. da Silva, and R. Mota, Nano Lett. **3**, 289 (2003).
[28]Y. V. Shtogun and L. M. Woods, Carbon **47**, 3252 (2009).
[29]A. Krishnan, E. Dujardin, T. W. Ebbesen, P. N. Yianilos, and M. M. J. Treacy, Phys. Rev. B **58**, 14013 (1998).
[30]M. F. Yu, B. S. Files, S. Arepalli, and R. S. Ruoff, Phys. Rev. Lett. **84**, 5552 (2000).
[31]T. W. Tombler, C. W. Zhou, L. Alexseyev, J. Kong, H. J. Dai, L. Lei, C. S. Jayanthi, M. Tang, and S.-Y. Wu, Nature (London) **405**, 769 (2000).
[32]Y. Jin and F. G. Yuan, Compos. Sci. Technol. **63**, 1507 (2003).
[33]T. Xiao and K. Liao, Phys. Rev. B **66**, 153407 (2002).
[34]P. M. Agrawal, B. S. Sudalayandi, L. M. Raff, and R. Komanduri, Comput. Mater. Sci. **38**, 271 (2006).
[35]E. Hernández, C. Goze, P. Bernier, and A. Rubio, Appl. Phys. A: Mater. Sci. Process. **68**, 287 (1999).
[36]C. F. Cornwell and L. T. Wille, Solid State Commun. **101**, 555 (1997).
[37]O. Gülseren, T. Yildirim, S. Ciraci, and C. Kilic, Phys. Rev. B **65**, 155410 (2002).
[38]J. P. Lu, Phys. Rev. Lett. **79**, 1297 (1997).
[39]Z. Xin, Z. Jianjun, and O.-Y. Zhong-can, Phys. Rev. B **62**, 13692 (2000).
[40]G. Kresse and J. Furthmuller, Phys. Rev. B **54**, 11169 (1996).
[41]G. Kresse and D. Joubert, Phys. Rev. B **59**, 1758 (1999).
[42]S. Berber and A. Oshiyama, Physica B **376–377**, 272 (2006).
[43]S. Bhagavantam, *Crystal Symmetry and Physical Properties* (Academic, London, 1966).
[44]K. Brugger, Phys. Rev. **133**, A1611 (1964).